Published in IET Radar, Sonar and Navigation
Received on 26th September 2008
Revised on 23rd April 2009
doi: 10.1049/iet-rsn.2008.0146

Special Issue – selected papers from IEEE RadarCon 2008

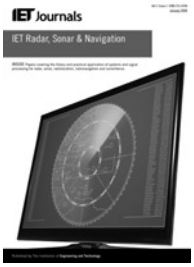

ISSN 1751-8784

Waveform design in signal-dependent interference and application to target recognition with multiple transmissions

R.A. Romero N.A. Goodman

Department of Electrical and Computer Engineering, The University of Arizona, 1230 E. Speedway Blvd, Tucson, AZ 85721, USA
E-mail: goodman@ece.arizona.edu

Abstract: The authors present illumination waveforms matched to stochastic targets in the presence of signal-dependent interference. The waveforms are formed by SNR and mutual information (MI) optimisation. We also use these waveforms in cognitive radar (CR) target identification application. In this application, the radar system attempts to identify a deterministic or random target using multiple transmissions. These transmissions are adaptively modified in response to previously received echoes. In addition, the authors present a new multi-band application of the CR platform.

1 Introduction

Cognitive radar (CR) is a new concept for the operation of radar systems. Haykin [1] has proposed CR as a technological solution for performance optimisation in resource-constrained and interference-limited environments. The 'intelligent' system proposed in [1] would have the capability to observe and learn from the said environment. Moreover, it is assumed that a CR will operate closed loop and that its transmit waveform will be adaptive. This leads to the investigation of waveforms that can be adapted in response to prior measurements in order to achieve objectives more efficiently. In this paper, we consider the design of waveforms for system or target identification in the presence of clutter and demonstrate the application of these designs to target recognition by a system performing multiple transmissions in an adaptive manner.

Closed loop or not, the design of transmit waveforms is critical to the performance of a radar system. Traditionally, pulsed and wideband chirp transmit waveforms are used. The use of wideband waveforms is motivated by the goal of obtaining a high-range resolution (HRR) profile of a target, which can then be compared to a template or processed further. Formation of an HRR profile, however, is not necessary for target identification. For example, suppose a radar is to distinguish between two targets and each target is known to have a strong resonance in a certain narrow band. If identification is truly our goal, then a more efficient use of system resources would be to focus the transmit energy into these two bands even though the ambiguity function (and, hence, reconstructured target range profile) would be poor by traditional considerations.

Addressing this idea of adaptive waveform design in 'resource-constrained and interference-limited environments', we focus here on the design of waveforms matched to extended targets in the presence of signal-dependent interference (clutter) under a transmit energy constraint. The design of illumination waveforms matched to an extended target has been considered by several others. One early contribution that we will exploit in this paper is [2]. In [2], two paradigms were treated. The first was to design a waveform that maximised detection of a known target in additive white Gaussian noise (AWGN). Since the performance of detecting a known signal in Gaussian noise is directly related to SNR, SNR was the criterion used to design the waveform. The second paradigm was to consider the maximisation of mutual information (MI) between a received waveform and a Gaussian ensemble of targets. In this case, since radar targets have finite extent, a true power spectral density (PSD) could not be used to characterise the ensemble. Instead, Bell introduced the

doi: 10.1049/iet-rsn.2008.0146

concept of a spectral variance. We will present here an interpretation of the spectral variance concept that relates the concept more clearly back to the PSD of a true random process.

Matched signal design in the presence of clutter has been treated in [3], where clutter was modelled as a zero-mean complex Gaussian process described by a PSD. Practical clutter modelling usually depends on the scenario being investigated. Here, we will continue to model clutter statistically as was in [3] and many other applications such as in space–time adaptive processing (STAP). In [3], signals matched to known extended targets were designed according to the SNR criterion. Since the clutter component of the received signal depended on the transmit waveform, the waveform solution was found by an iterative numerical technique that was not proved to converge to the optimal signal. In [4], signal design in clutter was considered from the detection perspective for a point target rather than an extended target. An earlier reference for signal design for clutter rejection is [5], and work on waveform design for imaging in the presence of clutter has been presented in [6]. Additional references on waveform design, but not necessarily for clutter environments, include [7–10]. Our own work on signal design by the MI criterion in signal-dependent clutter is presented in [11].

In [12], waveform designs by both the SNR and MI criteria were used to improve the performance of a closed-loop radar system performing target recognition. In [12], the targets were modelled by a known impulse response and the additive noise was AWGN. Adaptive waveform design was integrated with sequential hypothesis testing to form a closed-loop active sensor. The adaptive waveforms depended on functions of the target characteristics that changed as the probabilities of the target hypotheses were modified. Therefore with each transmission, the hypothesis probabilities were updated, which resulted in a new waveform for the next transmission. Sequential hypothesis testing was used to determine when the transmissions could be ceased while obtaining a desired error rate. Preliminary work on extending this closed-loop strategy to recognition of classes of targets was presented in [13].

Contributions of this paper include an analysis of waveform design by MI and SNR constraints in the presence of clutter, and application of these waveform designs in a closed-loop, or cognitive, radar system performing recognition of both deterministic and random targets. We also demonstrate how our closed-loop framework and waveform design techniques can be applied to a multi-band transmission system where the system must adaptively select which band to use for any single transmission.

This paper is organised in the following manner. In Section 2, we present the signal model assumed for this work and contributions in matched waveform design for signal-dependent clutter. In Section 3, we analyse the saturation of SNR and MI that can occur in the presence of signal-dependent clutter. Section 4 presents a discrete-time system model, which is then used to derive the probability density functions necessary for updating hypothesis probabilities in a closed-loop application. Section 5 presents performance results for the closed-loop system and Section 6 contains our conclusions.

2 Signal model and matched waveform design in signal-dependent interference

2.1 Random extended target and the spectral variance

The block diagram in Fig. 1 represents the complex-valued baseband signal model being considered. Let $x(t)$ be a finite-energy waveform with duration T. Let $\boldsymbol{g}(t)$ be a zero-mean complex Gaussian random process with PSD $P_g(f)$. The clutter $\boldsymbol{c}(t)$ is a zero-mean complex Gaussian random process with spectral density $\boldsymbol{P}_c(f)$, and $\boldsymbol{n}(t)$ is the zero-mean receiver noise process with PSD $P_n(f)$.

Since a practical target has finite extent, consider a random extended target created by multiplying the random process $\boldsymbol{g}(t)$ with a rectangular window function of duration T_g. We denote this finite-extent random target as $\boldsymbol{g}_x(t)$. Since $\boldsymbol{g}_x(t)$ is not a true stationary Gaussian process, it cannot be characterised by a PSD. However, an energy spectral density (ESD) can be defined. If we let $\boldsymbol{G}(f)$ be the random transfer function corresponding to the Fourier transform of $\boldsymbol{g}_x(t)$, then the ESD is given by

$$\xi_{\mathrm{G}}(f) = E\left[|\boldsymbol{G}(f)|^2\right] \tag{1}$$

We can also define a mean and variance according to

$$\mu_{\mathrm{G}}(f) = E\left[\boldsymbol{G}(f)\right] \tag{2}$$

and the variance is

$$\sigma^2_{\mathrm{G}}(f) = E\left[|\boldsymbol{G}(f) - \mu_{\mathrm{G}}(f)|^2\right] \tag{3}$$

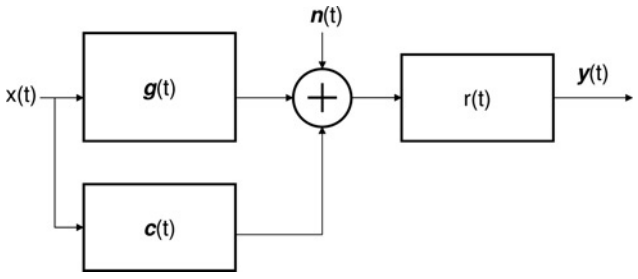

Figure 1 *Complex baseband signal model with random target in signal-dependent interference*

We refer to the variance in (3) as the energy spectral variance (ESV), and for the zero-mean processes assumed in this derivation, the ESV and ESD are the same.

Although not stationary over all time, $\boldsymbol{g}_x(t)$ is stationary in the support T_g. Hence, we can define an average power, valid in the support T_g. Based on the ESV, this average power is

$$\Upsilon_{\mathrm{G}}(f) = \frac{\sigma_{\mathrm{G}}^2(f)}{T_g} \tag{4}$$

which we call the power spectral variance (PSV). For the convolution of any known signal with this random process, we may also define spectral variances for the convolution output. If we define $\boldsymbol{z}(t)$ as the convolution of $x(t)$ with $\boldsymbol{g}_x(t)$, then the PSV for this convolution is defined as

$$\Upsilon_Z(f) = \frac{\sigma_{\mathrm{G}}^2(f)|X(f)|^2}{T_z} \tag{5}$$

where the numerator is the ESV and $T_z = T_g + T$. That is, the output PSV is defined as the time-averaged ESV of the output where the averaging interval is equal to the finite duration of the output. Of course, the instantaneous average power of the convolution between two finite-duration signals changes with time, so the PSV should not be interpreted as describing an average power that is constant over the interval T_z. Both the ESV and PSV will play roles in our derivations of waveforms matched to random targets of finite duration.

Referring back to Fig. 1, the output signal $\boldsymbol{y}(t)$ is given by

$$\boldsymbol{y}(t) = r(t) * [x(t) * \boldsymbol{g}_x(t) + x(t) * \boldsymbol{c}(t) + \boldsymbol{n}(t)] \tag{6}$$

Let $\boldsymbol{y}_s(t)$ and $\boldsymbol{y}_n(t)$ be the output signal and noise components given by

$$\boldsymbol{y}_s(t) = r(t) * [x(t) * \boldsymbol{g}_x(t)] \tag{7}$$

and

$$\boldsymbol{y}_n(t) = r(t) * [x(t) * \boldsymbol{c}(t) + \boldsymbol{n}(t)] \tag{8}$$

respectively.

2.2 SNR waveform derivation

The power of the signal component at time t is

$$E[|\boldsymbol{y}_s(t)|^2] = \int_{-\infty}^{\infty}\int_{-\infty}^{\infty} R(f)R^*(-\gamma)X(f)X^*(-\gamma) \times E[\boldsymbol{G}(f)\boldsymbol{G}^*(-\gamma)]\, \mathrm{e}^{\mathrm{j}2\pi(f+\gamma)t}\, \mathrm{d}\gamma\, \mathrm{d}f \tag{9}$$

If $\boldsymbol{g}_x(t)$ were a true random process, then its frequency-domain coefficients at different frequencies would be uncorrelated. However, since the target has finite duration, its frequency-domain coefficients are correlated, which means that the signal power at the output of the receive filter varies with time. If we assume, however, that both T and T_r are much less than T_g, then there exists a finite duration of time during which the transmit waveform and receive filter overlap the finite-duration target by the same amount. During this window, the average power is constant. Thus, the average power during this interval is

$$E[|\boldsymbol{y}_s(t)|^2] \simeq \int_{-\infty}^{\infty} |R(f)|^2|X(f)|^2\sigma_{\mathrm{G}}^2(f)\, \mathrm{d}f \tag{10}$$

For some time t_0 during this interval, we define SNR to be the ratio of the average power of the signal component to the average power of the noise and interference component. Thus, SNR is defined as

$$(\mathrm{SNR})_{t_0} \equiv \frac{E[|\boldsymbol{y}_s(t_0)|^2]}{E[|\boldsymbol{y}_n(t_0)|^2]} \tag{11}$$

The interference power is

$$E[|\boldsymbol{y}_n(t_0)|^2] = \int_{-\infty}^{\infty} P_N(f)\, \mathrm{d}f = \int_{-\infty}^{\infty} |R(f)|^2 L(f)\, \mathrm{d}f \tag{12}$$

where $L(f)$ is given by

$$L(f) = |X(f)|^2 P_g(f) + P_n(f) \tag{13}$$

Thus, the approximated SNR is

$$(\mathrm{SNR})_{t_0} = \frac{\int_{-\infty}^{\infty} |R(f)|^2\sigma_{\mathrm{G}}^2(f)|X(f)|^2\, \mathrm{d}f}{\int_{-\infty}^{\infty} |R(f)|^2 L(f)\, \mathrm{d}f} \tag{14}$$

Maximisation of (14) over $|X(f)|^2$ presents a difficulty since it is dependent on both $X(f)$ and $R(f)$. However, we can define an upper bound on SNR according to

$$(\mathrm{SNR})_{t_0} < B_{\mathrm{SNR}} = \frac{\left|\int_{-\infty}^{\infty} |R(f)|\sqrt{L(f)}\left(\sqrt{\sigma_G^2(f)}|X(f)|/\sqrt{L(f)}\right)\, \mathrm{d}f\right|^2}{\int_{-\infty}^{\infty} |R(f)|^2 L(f)\, \mathrm{d}f} \tag{15}$$

Straightforward application of Schwarz's inequality to (15) results in a receive filter of the form

$$|R(f)| = k\frac{\sqrt{\sigma_{\mathrm{G}}^2(f)}|X(f)|}{|X(f)|^2 P_c(f) + P_n(f)} \tag{16}$$

where k is a proportionality constant. For a waveform with energy concentrated in the band $[-W/2, W/2]$, the SNR bound equation to be maximised, under the energy constraint

$$\int_W |X(f)|^2\, \mathrm{d}f \le E_x \tag{17}$$

doi: 10.1049/iet-rsn.2008.0146

is now given by

$$B_{\mathrm{SNR}} \simeq \int_W \frac{\sigma_{\mathrm{G}}^2(f)|X(f)|^2}{P_c(f)|X(f)|^2 + P_n(f)}\,\mathrm{d}f \tag{18}$$

Application of the Lagrangian multiplier technique maximises (18) with respect to $|X(f)|^2$, which leads to the optimum waveform spectrum described by

$$|X(f)|^2 = \max\left[0,\ \frac{\sqrt{\sigma_{\mathrm{G}}^2(f)P_n(f)}}{P_c(f)}\left(A - \sqrt{\frac{P_n(f)}{\sigma_{\mathrm{G}}^2(f)}}\right)\right] \tag{19}$$

where A is a constant determined by the energy constraint

$$\int_W \max\left[0,\ \frac{\sqrt{\sigma_{\mathrm{G}}^2(f)P_n(f)}}{P_c(f)}\left(A - \sqrt{\frac{P_n(f)}{\sigma_{\mathrm{G}}^2(f)}}\right)\right]\mathrm{d}f \le E_x \tag{20}$$

In the case where clutter is absent, B_{SNR} reduces to

$$B_{\mathrm{SNR}} = \int_{-\infty}^{\infty} \frac{\sigma_{\mathrm{G}}^2(f)}{P_n(f)}|X(f)|^2\,\mathrm{d}f \tag{21}$$

It can be shown that the finite-duration, energy-constrained $x(t)$ that maximises (21) is given by the primary eigenfunction of

$$\lambda_{\max}\check{x}(t) = \int_{-T/2}^{T/2} \check{x}(\tau)R_g(t-\tau)\,\mathrm{d}\tau \tag{22}$$

where the kernel $R_g(t)$ is

$$R_g(t) = \int_{-\infty}^{\infty} \frac{\sigma_{\mathrm{G}}^2(f)}{P_n(f)}\,\mathrm{e}^{\mathrm{j}2\pi ft}\,\mathrm{d}f \tag{23}$$

For complex-valued white noise, (23) becomes

$$R_g(t) = \frac{1}{N_0}\int_{-\infty}^{\infty} \sigma_{\mathrm{G}}^2(f)\,\mathrm{e}^{\mathrm{j}2\pi ft}\,\mathrm{d}f \tag{24}$$

2.3 Derivation of MI waveforms

Consider again the signal model of Fig. 1. For the MI waveform derivation, we treat the receiver filter as an ideal lowpass filter (LPF) with approximate time duration $T_r \ll T$ and $T_r \ll T_g$. Therefore T_r can be effectively ignored, and the receive filter simply becomes an explicit statement that the radar system is band limited [2].

We wish to derive a waveform that optimises the MI between the received waveform $\boldsymbol{y}(t)$ and the random target $\boldsymbol{g}(t)$. If the target were a true, infinite-duration random process with PSD $P_g(f)$, then the entropy of the target random process would be infinite because it would have finite variance for an infinite duration of time. In this case, we could define an MI rate according to

$$\dot{I}(\boldsymbol{y}(t);\boldsymbol{g}(t)|x(t)) = \int_W \ln\left[1 + \frac{|X(f)|^2P_g(f)}{\{P_n(f) + |X(f)|^2P_c(f)\}}\right]\mathrm{d}f \tag{25}$$

and the MI obtained in a time interval of duration T would be

$$I(\boldsymbol{y}(t);\boldsymbol{g}(t)|x(t)) = T\dot{I}(\boldsymbol{y}(t);\boldsymbol{g}(t)|x(t)) \tag{26}$$

However, in our application the target is characterised by the finite-duration signal $\boldsymbol{g}_x(t)$ with PSV $\Upsilon_{\mathrm{G}}(f) = \sigma_{\mathrm{G}}^2(f)/T_g$. To obtain an MI expression useful for a random, finite-duration target, we substitute the time-averaged PSV (4) for the PSD of a random process. Let T_z be the duration of the convolution of the transmit waveform and the target response, that is, $T_z = T + T_g$. Using the PSV of the signal output defined earlier, the approximate MI applicable to the finite-duration target is

$$\begin{aligned} &I(\boldsymbol{y}(t);\boldsymbol{g}_x(t)|x(t)) \\ &\quad\simeq T_z\int_W \ln\left[1 + \frac{|X(f)|^2\sigma_{\mathrm{G}}^2(f)}{T_z\{P_n(f) + |X(f)|^2P_c(f)\}}\right]\mathrm{d}f \\ &\quad= T_z\int_W \ln\left[1 + \left\{\frac{\alpha|X(f)|^2\Upsilon_{\mathrm{G}}(f)}{P_n(f) + |X(f)|^2P_c(f)}\right\}\right]\mathrm{d}f \end{aligned} \tag{27}$$

where $\alpha = T_g/T_z$.

Realising that the kernel of (27) is a concave function, maximisation with respect to $|X(f)|^2$ under the energy constraint (17) yields

$$|X(f)|^2 = \max\left[0,\ -U(f) + \sqrt{U^2(f) + S(f)(A - D(f))}\right] \tag{28}$$

where

$$D(f) = \frac{P_n(f)}{\alpha\Upsilon_{\mathrm{G}}(f)} \tag{29}$$

$$U(f) = \frac{P_n(f)(2P_c(f) + \alpha\Upsilon_{\mathrm{G}}(f))}{2P_c(f)(P_c(f) + \alpha\Upsilon_{\mathrm{G}}(f))} \tag{30}$$

and

$$S(f) = \frac{P_n(f)\alpha\Upsilon_{\mathrm{G}}(f)}{P_c(f)(P_c(f) + \alpha\Upsilon_{\mathrm{G}}(f))} \tag{31}$$

The constant A is determined by the energy constraint

$$\int_W \max\left[0,\ -U(f)+\sqrt{U^2(f)+S(f)(A-D(f))}\right]\mathrm{d}f \le E_x \tag{32}$$

When clutter is absent, the optimum waveform spectrum becomes

$$|X(f)|^2 = \max\left[0, A-\frac{P_n(f)}{\alpha \Upsilon_{\mathrm{G}}(f)}\right] \tag{33}$$

where A is again controlled by the energy constraint.

To obtain a final expression for MI for a finite-duration random target, we implicitly made the assumption that $T_g \gg T$. This assumption is equivalent to approximating the random target's frequency-domain coefficients to be uncorrelated such that the MI can be obtained by integrating over the frequency spectrum. This assumption was made when we substituted the PSV for the PSD of a true random process. In the expression that results, if we indeed let $T_g \to \infty$, then $\boldsymbol{g}_x(t)$ becomes the true random process $\boldsymbol{g}(t)$, the constant $\alpha \to 1$, and the integral in (27) converges to (25), which is consistent with the result derived in [2].

3 SNR and MI saturation in signal-dependent interference

In the presence of clutter, the SNR or MI obtained by the optimum waveform eventually saturates such that no additional benefit is obtained by transmitting more energy. This occurs for high transmit energy because the measurements become clutter limited rather than noise limited. Because the clutter is signal dependent, the system eventually arrives at the point where additional transmit energy increases the received clutter power just as much as it does the received signal power. However, the two transmit waveforms have different strategies for distributing the transmit energy, which has been observed before in [12]. Therefore the waveforms saturate at different energy levels.

To understand the saturation that occurs, recall the kernel expressions in (18) and (27). If we take the derivative of each kernel with respect to the transmit spectrum $|X(f)|^2$, we obtain

$$K'_{B_{\mathrm{SNR}}}(f) = \frac{\sigma^2_{\mathrm{G}}(f)P_n(f)}{[P_c(f)|X(f)|^2+P_n(f)]^2} \tag{34}$$

and

$$K'_I(f) = \frac{\alpha P_n(f)\Upsilon_{\mathrm{G}}(f)}{P_n^2(f)+A(f)|X(f)|^2+B(f)(|X(f)|^2)^2} \tag{35}$$

where

$$A(f) = 2P_n(f)P_c(f)+P_n(f)\alpha\Upsilon_{\mathrm{G}}(f) \tag{36}$$

and

$$B(f) = P_c^2(f)+\alpha\Upsilon_{\mathrm{G}}(f)P_c(f) \tag{37}$$

Considering both (34) and (35), we see that the derivatives go to zero as the transmit energy becomes large, for all frequencies. This means that the SNR and MI obtained will eventually plateau as energy increases.

Fig. 2 shows the derivatives of the SNR and MI kernel functions at three different frequencies for a sample scenario. The derivatives all approach zero for large transmit energy, although they converge to zero at different rates and energies depending on the clutter and target spectra at an individual frequency.

4 Application to CR

In this section, we will present application results of the SNR and MI waveform designs to a closed-loop radar system. In particular, we explore the target recognition or discrimination problem. We first present a discrete-time model that facilitates pdf expressions as well as computer simulation. We also derive pdf expressions that will be used in the closed-loop transmission scheme to update

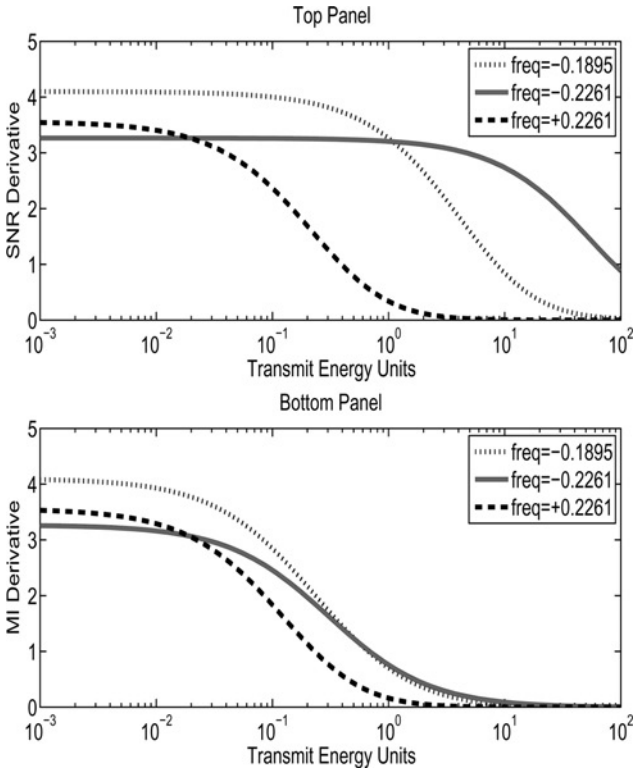

Figure 2 *MI and SNR kernel derivatives of three frequency points of a sample target–clutter–noise scenario*

doi: 10.1049/iet-rsn.2008.0146

hypothesis probabilities without the need to retain the data from previous transmissions. We then describe a closed-loop radar platform designed for target class identification. Finally, we present the results from simulations designed to assess the performance of our waveform designs in the closed-loop system. Performance metrics include error rates or the average number of illuminations required for a desired error rate. We also present a multi-band demonstration of the CR framework.

4.1 Discrete signal model

We define the sampling interval of our discrete-time model to be a normalised value of $T_s = 1$. Define $\boldsymbol{g}$ as the complex-Gaussian-distributed target vector of length L that is obtained by sampling the random target function $\boldsymbol{g}_x(t)$. Similarly, let $\boldsymbol{x}$ be the length-L_x transmit signal vector with energy

$$E_{\boldsymbol{x}} = \boldsymbol{x}^{\mathrm{H}}\boldsymbol{x} \tag{38}$$

Thus, the length-L_y received signal vector $\boldsymbol{y}$ is given by

$$\boldsymbol{y} = \boldsymbol{g} * \boldsymbol{x} + \boldsymbol{c} * \boldsymbol{x} + \boldsymbol{n} \tag{39}$$

where the length-L complex Gaussian vector $\boldsymbol{g}$ has covariance $\boldsymbol{K}_{\boldsymbol{g}}$ and $\boldsymbol{c}$ is the complex Gaussian length-L clutter process with covariance $\boldsymbol{K}_{\boldsymbol{c}}$. If we define a transmit signal convolution matrix of size $L_y \times L$ given by

$$\boldsymbol{X} = \begin{bmatrix} x(1) & 0 & \cdots & \cdots & 0 \\ x(2) & x(1) & \ddots & \cdots & 0 \\ \vdots & \vdots & \ddots & \ddots & \vdots \\ x(L_x) & x(L_x-1) & \cdots & x(1) & 0 \\ 0 & x(L_x) & x(L_x-1) & \cdots & x(1) \\ \vdots & 0 & x(L_x) & \cdots & x(2) \\ \vdots & \vdots & 0 & \ddots & \vdots \\ 0 & 0 & \cdots & 0 & x(L_x) \end{bmatrix} \tag{40}$$

then the length-L_y received signal vector is then

$$\boldsymbol{y} = \boldsymbol{X}\boldsymbol{g} + \boldsymbol{X}\boldsymbol{c} + \boldsymbol{n} \tag{41}$$

where $L_y = L_x + L - 1$. For multiple transmissions, the measurements due to the Kth transmission are

$$\boldsymbol{y}_K = \boldsymbol{X}_K\boldsymbol{g} + \boldsymbol{X}_K\boldsymbol{c} + \boldsymbol{n}_K \tag{42}$$

Note that the transmit waveform matrix has a subscript K, which is consistent with the idea that the waveform will adapt on each transmission.

4.2 Target–clutter scenarios in closed-loop system

In a closed-loop radar environment where measurements collected on subsequent transmissions may or may not be correlated, different target and clutter scenarios are possible. We consider four scenarios and derive the underlying joint pdf of the measurements collected over multiple transmissions. In each case, the pdf's can be calculated by accumulating results from previous transmissions. This is important because the idea of cognitive radar is to represent the radar channel in a probabilistic manner, to update the probabilities and radar channel hypotheses as data are received, and to adapt the transmission and measurement strategy accordingly. If, in order to update the radar's probabilistic understanding of the radar channel, old measurements must be retained, data storage requirements will quickly become untenable. The requisite pdf for a correlated target impulse response vector $\boldsymbol{g}$ in the absence of clutter is derived in detail in Appendix. The following scenarios require straightforward modifications of the approach in Appendix. When we say that the target and/or clutter is correlated, we mean that the target and/or clutter impulse response vector ($\boldsymbol{g}$ and/or $\boldsymbol{c}$) is a realisation of a complex Gaussian random vector, but the realisation does not change between transmissions. This is a good model for scenarios where the target and radar are stationary. If the target and/or radar move significantly between transmissions, then a better model is to generate independent realisations of these random vectors for each transmission.

1. *Deterministic target and correlated clutter:* For a target that is deterministic and a clutter realisation that is perfectly correlated from transmission to transmission, the joint pdf of the measurements under a given hypothesis is given by

$$p(\boldsymbol{y}_1, \ldots, \boldsymbol{y}_K) = \frac{|\boldsymbol{Q}^{-1}|}{|\boldsymbol{K}_{\boldsymbol{c}}|\pi^{LK}|\boldsymbol{K}_{\boldsymbol{N}}|^K} \exp\left[-\sum_{k=1}^{K}[\hat{\boldsymbol{y}}_k]^{\mathrm{H}}\boldsymbol{K}_{\boldsymbol{N}}{}^{-1}[\hat{\boldsymbol{y}}_k]\right] \times \exp\left[\left[\sum_{k=1}^{K}\boldsymbol{X}_k^{\mathrm{H}}\boldsymbol{K}_{\boldsymbol{N}}{}^{-1}[\hat{\boldsymbol{y}}_k]\right]^{\mathrm{H}}\boldsymbol{Q}^{-1}\sum_{k=1}^{K}\boldsymbol{X}_k^{\mathrm{H}}\boldsymbol{K}_{\boldsymbol{N}}{}^{-1}[\hat{\boldsymbol{y}}_k]\right] \tag{43}$$

where

$$\hat{\boldsymbol{y}}_{\boldsymbol{k}} = \boldsymbol{y}_k - \boldsymbol{X}_k\boldsymbol{g} \tag{44}$$

$$\boldsymbol{Q} = \boldsymbol{K}_{\boldsymbol{c}}^{-1} + \sum_{k=1}^{K}\boldsymbol{X}_k^{\mathrm{H}}\boldsymbol{K}_{\boldsymbol{N}}^{-1}\boldsymbol{X}_k \tag{45}$$

2. *Correlated target and independent clutter:* For a scenario where the target realisation remains the same and the clutter realisation changes from transmission to transmission, the joint pdf of the measurements under a

given hypothesis is

$$p(\boldsymbol{y}_1, \ldots, \boldsymbol{y}_K) = \frac{|\boldsymbol{Q}^{-1}|}{|\boldsymbol{K}_g|\pi^{LK}|\boldsymbol{K}_N|^K} \exp\left[-\sum_{k=1}^{K} \boldsymbol{y}_k^{\mathrm{H}} \boldsymbol{K}^{-1} \boldsymbol{y}_k\right] \times \exp\left[\left[\sum_{k=1}^{K} \boldsymbol{X}_k^{\mathrm{H}} \boldsymbol{K}^{-1} \boldsymbol{y}_k\right]^{\mathrm{H}} \boldsymbol{Q}^{-1} \sum_{k=1}^{K} \boldsymbol{X}_k^{\mathrm{H}} \boldsymbol{K}^{-1} \boldsymbol{y}_k\right] \quad (46)$$

where $\boldsymbol{K}$ and $\boldsymbol{Q}$ are defined by

$$\boldsymbol{K} = \boldsymbol{K}_N + \boldsymbol{X}_k^{\mathrm{H}} \boldsymbol{K}_c \boldsymbol{X}_k \quad (47)$$

$$\boldsymbol{Q} = \boldsymbol{K}_g^{-1} + \sum_{k=1}^{K} \boldsymbol{X}_k^{\mathrm{H}} \boldsymbol{K}_N{}^{-1} \boldsymbol{X}_k \quad (48)$$

3. *Independent target, clutter and noise:* For a scenario where the target and clutter realisations are independent from transmission to transmission, the joint pdf of the measurements under a given hypothesis is

$$p(\boldsymbol{y}_1, \ldots, \boldsymbol{y}_K) = \frac{1}{\pi^{LK}|\boldsymbol{K}_N + \boldsymbol{X}_k^{\mathrm{H}} \boldsymbol{K}_f \boldsymbol{X}_k|^K} \times \exp\left[-\sum_{k=1}^{K} \boldsymbol{y}_k^{\mathrm{H}} (\boldsymbol{K}_N + \boldsymbol{X}_k^{\mathrm{H}} \boldsymbol{K}_f \boldsymbol{X}_k)^{-1} \boldsymbol{y}_k\right] \quad (49)$$

where $\boldsymbol{K}_f$ is given by

$$\boldsymbol{K}_f = \boldsymbol{K}_c + \boldsymbol{K}_g \quad (50)$$

4. *Correlated target and correlated clutter:* In the case where both target and clutter realisations remain constant over all transmissions, the joint pdf after the Kth observation is

$$p(\boldsymbol{y}_1, \ldots, \boldsymbol{y}_K) = \frac{|\boldsymbol{Q}^{-1}|}{|\boldsymbol{K}_t|\pi^{LK}|\boldsymbol{K}_N|^K} \exp\left[-\sum_{k=1}^{K} \boldsymbol{y}_k^{\mathrm{H}} \boldsymbol{K}_N^{-1} \boldsymbol{y}_k\right] \times \exp\left[\left[\sum_{k=1}^{K} \boldsymbol{X}_k^{\mathrm{H}} \boldsymbol{K}_N^{-1} \boldsymbol{y}_k\right]^{\mathrm{H}} \boldsymbol{Q}^{-1} \sum_{k=1}^{K} \boldsymbol{X}_k^{\mathrm{H}} \boldsymbol{K}_N^{-1} \boldsymbol{y}_k\right] \quad (51)$$

where $\boldsymbol{K}_t$ and $\boldsymbol{Q}$ are defined by

$$\boldsymbol{K}_t = \boldsymbol{K}_g + \boldsymbol{K}_c \quad (52)$$

$$\boldsymbol{Q} = \boldsymbol{K}_t^{-1} + \sum_{k=1}^{K} \boldsymbol{X}_k^{\mathrm{H}} \boldsymbol{K}_N^{-1} \boldsymbol{X}_k \quad (53)$$

Again, the correlated-target case in a clutter-free environment is derived in detail in Appendix.

4.3 Target class identification

In [12], a closed-loop radar system in AWGN was proposed for target identification of known target responses. Fig. 3 represents the application of the CR platform in [12] to a signal-dependent environment. Consider a target identification problem in which a target from one of M possible target classes is present. A Bayesian representation of the channel is formulated where the target hypotheses are denoted by $H_1, H_2, \ldots, H_M$ with corresponding prior probabilities $P_1, P_1, \ldots, P_M$. The ith hypothesis is characterised by a random target ensemble $\boldsymbol{g}_i(t)$ with a corresponding ESV $\sigma^2_{\mathrm{G},i}(f)$, $i = 1, 2, \ldots, M$. The random clutter realisation $\boldsymbol{c}(t)$ is also illuminated and received as signal-dependent interference. Since the target is a realisation of a Gaussian target class, the actual target impulse response is unknown a priori. Thus, the application is that of a target class identification problem, that is, we try to identify which stochastic ensemble the target realisation belongs to despite interference because of received noise and signal-dependent clutter.

The first step for CR operation is to determine how to translate from the waveforms derived above to a waveform that performs well for the multiple-hypothesis identification problem. Application of the matched waveforms should depend on the hypothesis probabilities such that the waveform will change in response to understanding of the classification problem obtained from prior transmissions. Similar to what was proposed in [12] for deterministic targets, we calculate a probability-weighted spectral variance

$$P_{\mathrm{G}}(f) = \sum_{i=1}^{M} \Pr(H_i)\sigma^2_{\mathrm{G},i}(f) - \left|\sum_{i=1}^{M} \Pr(H_i)\sqrt{\sigma^2_{\mathrm{G},i}(f)}\right|^2 \quad (54)$$

which may be thought of as an effective ESV over multiple target classes. Depending on the waveform of choice, the optimum waveform is obtained by substituting (54) into either (19) for an SNR-based waveform or (28) for an MI-based waveform.

After each transmission, the CR system updates the hypothesis probabilities by processing the received echo.

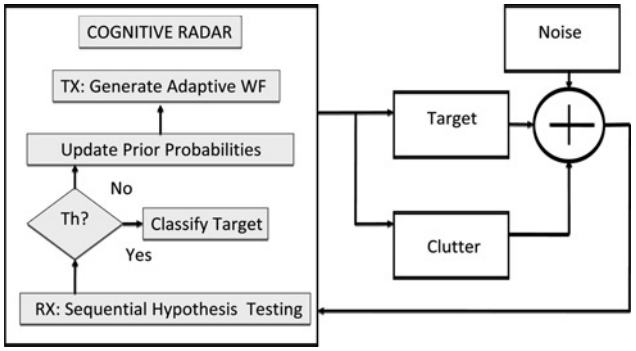

Figure 3 *Block diagram of a closed-loop radar system*

doi: 10.1049/iet-rsn.2008.0146

Depending on the target and clutter model, the data due to the current transmission are substituted into one of the joint pdf's from Section 4.2. For target hypothesis H_i, the update rule is

$$P_i^{K+1} = \beta p_K(\boldsymbol{y}_1, \boldsymbol{y}_2, \ldots, \boldsymbol{y}_K) P_i \tag{55}$$

where β ensures unity probability over the classes at each iteration.

Once the probabilities are updated, a new spectral variance function is calculated, which results in a new waveform for the next transmission. This closed-loop procedure continues either for a fixed number of transmissions or for deterministic target hypotheses, until all the pairwise likelihood ratios meet thresholds defined by a multi-hypothesis sequential hypothesis test.

5 Results

5.1 Closed-loop radar

We now present performance results based on simulated scenarios. For scenarios involving random target realisations, we allow the closed-loop system to perform ten transmissions and receptions, then select the target class with the highest probability as the system's decision. Indeed, in some practical systems, the number of transmissions is fixed. Error rates are shown as a function of the energy constraint per illumination for various waveform strategies. For deterministic targets, we perform Monte Carlo simulation to obtain the average number of illuminations required to make a decision with specified confidence. This transmission approach models flexible systems that allow for the number of illuminations to vary.

Fig. 4 shows the probability of misclassification for a scenario where the clutter and target realisations are both perfectly correlated over the ten transmissions of the experiment. Four target classes were defined, and each class was characterised by a PSV with energy concentrated into narrow frequency bands. These bands did not overlap with each other or with the spectral bands of the other classes. The clutter PSD was a smooth spectrum with most of the power concentrated in the middle half of the band. Each target had approximately one band located in strong clutter and one band located in weak clutter. In Fig. 4, the target-to-noise ratio (TNR), defined by the ratio of the area under the target PSV to the average power of the receiver noise, was 3 dB. The clutter-to-noise ratio (CNR), defined by the ratio of the area under the clutter PSD to the receiver noise power, was 8 dB. One can see from the plot that the two waveforms that accounted for the clutter PSD performed better than the two waveforms that did not account for clutter, even in this scenario with relatively weak clutter. The 'MI w/o clutter' designation denotes the MI waveform designed with the clutter PSD set to zero. The wideband waveform has evenly distributed energy over the transmission

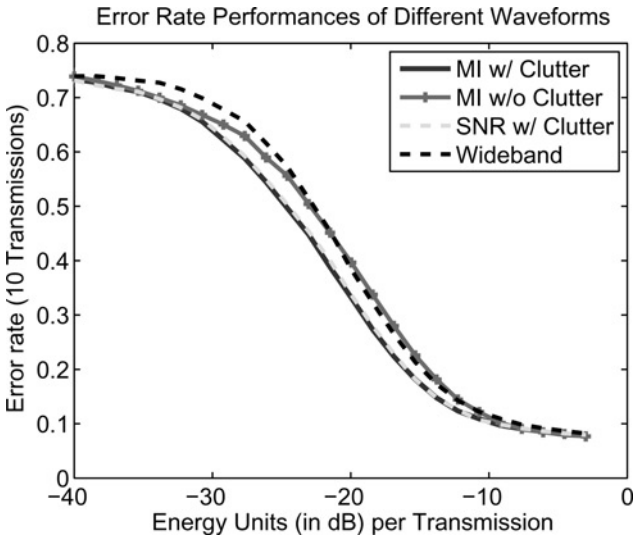

Figure 4 *Error rates for classification of random targets with correlated measurements*

band. Note the existence of an error floor at higher transmit energies. This floor is due to the fact that target realisations from the different classes are not mutually exclusive, so realisations from one class may actually look like they should be from another class. This effect is exacerbated by the presence of clutter and by the fact that the received echos are correlated across transmissions.

Fig. 5 shows results for the same type of experiment, except that new target and clutter realisations were

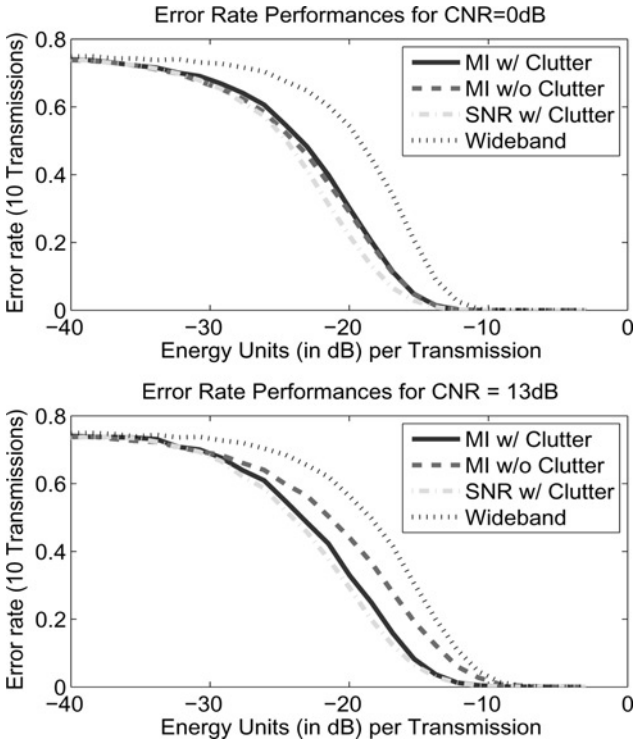

Figure 5 *Error rates for classification of random targets with independent measurements*

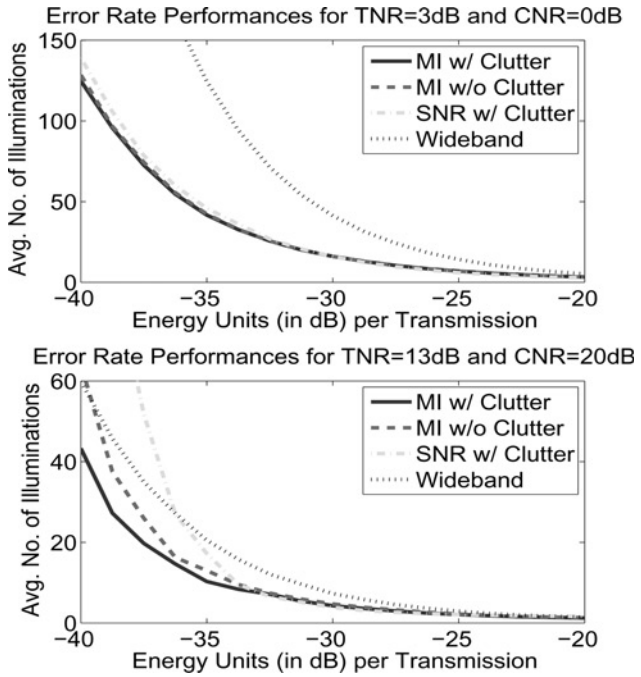

Figure 6 *Average number of illuminations to identify deterministic targets*

independently generated for each transmission. As we would expect, performance is better for this case compared to the correlated case because multiple target and clutter realisations are observed. Consider the bottom panel of Fig. 5 where TNR = 3 dB and CNR = 13 dB. Despite the fact that the clutter power is stronger than that of Fig. 4, observing multiple realisations of the target has removed

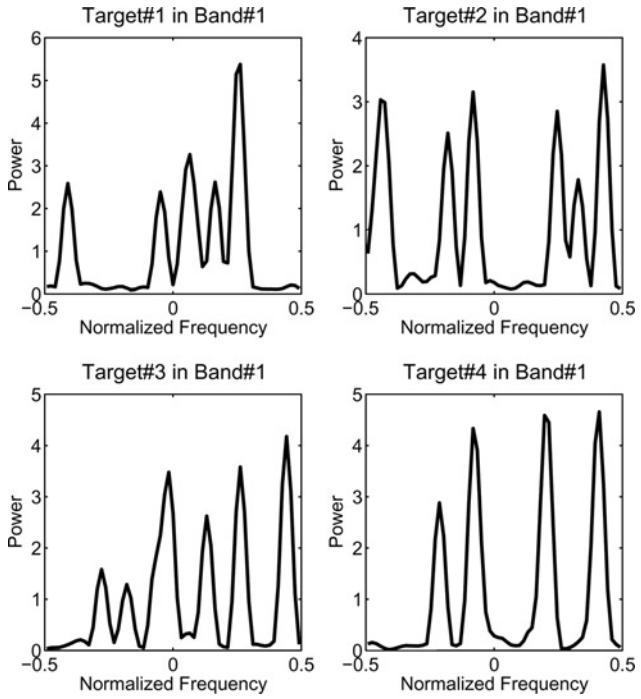

Figure 7 *Four target PSVs corresponding to four hypotheses in Band #1*

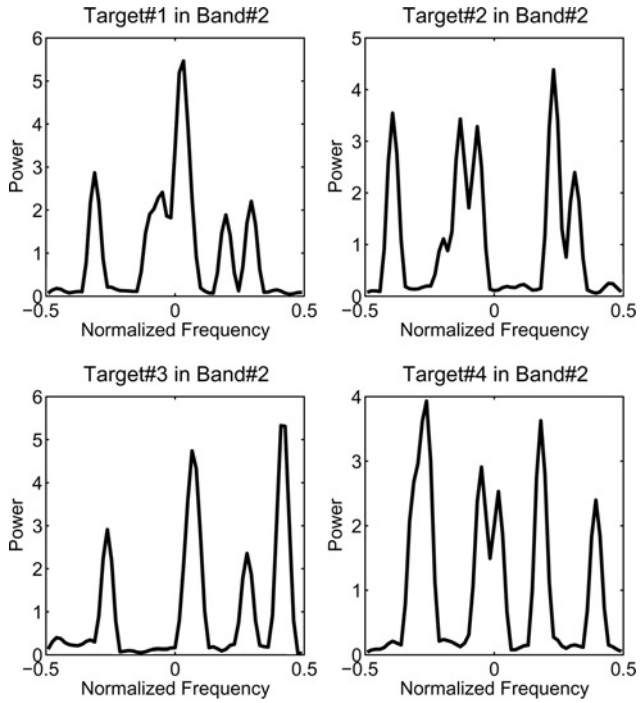

Figure 8 *Four target PSVs corresponding to four hypotheses in Band #2*

the floor in performance. The top panel of Fig. 5 shows the performances of the different waveforms where TNR = 3 dB and CNR = 0 dB, that is, the system is not clutter limited. Notice the modest performance gain of the waveforms that compensate for clutter. Recall the bottom panel of Fig. 5, where the scenario is clutter limited with CNR = 13 dB. Here, the waveforms that account for clutter clearly outperform the waveforms that do not account for clutter. Thus, performance of clutter-compensating waveforms improve with increasing CNR.

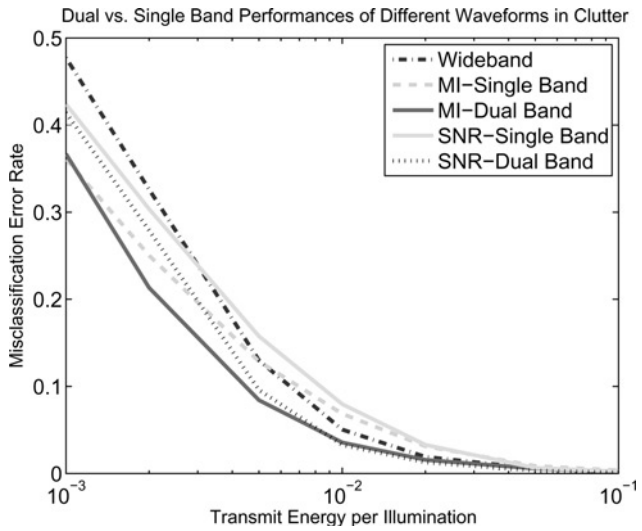

Figure 9 *Error rate performances of various single-band and dual-band waveforms*

doi: 10.1049/iet-rsn.2008.0146

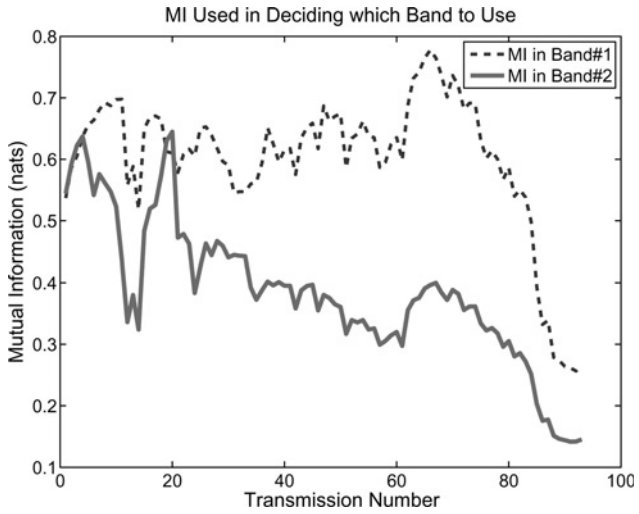

Figure 10 *MI calculations on both bands prior to transmission*

In Fig. 6, we switch to a scenario where the target impulse responses are assumed to be known. Multiple realisations of the target impulse responses are generated over the course of the Monte Carlo simulation, but once the realisations are generated for each hypothesis, they are treated as known for that particular trial. In this case, since the targets are deterministic and known, the target classes are mutually exclusive and we can apply sequential hypothesis testing to control the error rate. Sequential hypothesis testing is a technique where thresholds for the likelihood ratios can be defined such that the system only stops taking measurements when the thresholds are met. The thresholds can be chosen to achieve a desired error rate, but for any given trial, the number of observations necessary to achieve the threshold is a random number. We set the probability of error to 0.05 and performed Monte Carlo simulation of 20 000 trials for each transmit energy level. Then the average number of illuminations was calculated and plotted against transmit energy. Thus, waveforms that use fewer

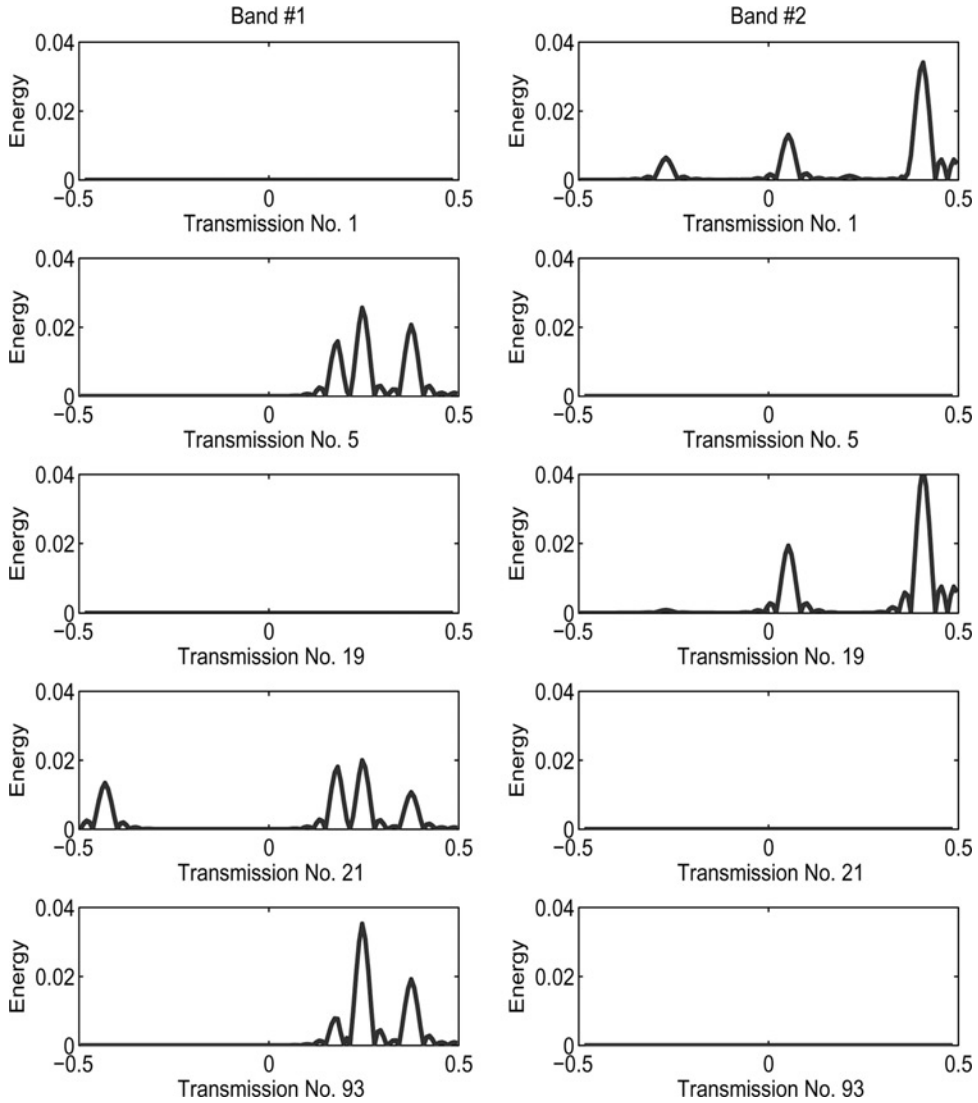

Figure 11 *Few select transmission waveforms in a single experiment of a dual-band CR*

average transmissions can be said to use their energy more efficiently. Again, the MI and SNR waveforms designed for signal-dependent clutter are the best performers, with a notable exception. At low transmit energy, the SNR-based waveform tends to perform poorly – even worse than the wideband waveform that uses no prior knowledge of the target spectra. The SNR waveform is known to focus all or most of its energy into a single narrow frequency band. Apparently, this is not a good strategy for this scenario.

5.2 Multi-band application

For targets of very short duration, that is, with large bandwidths, it may not be practical for a radar system to match the whole bandwidth in a single transmission. However, some practical radar systems are equipped with dual bands, but may only use one band at a time. We now demonstrate CR under this practical constraint using the same MI and SNR design metrics as before. First, we define $M = 4$ target ensemble classes. Their arbitrarily generated PSVs in two separate bands are shown in Figs. 7 and 8. A lowpass-shaped PSD in each frequency band is used to model the clutter. In this experiment, we will consider the difficult case where the measurements are correlated because of both the target and clutter realisations remaining fixed over the transmissions. Five transmit waveform types are used; an impulse waveform denoted by 'wideband', the optimum MI waveform in clutter using a single band, the optimum MI waveform in clutter utilising both bands, the SNR waveform in a single band and the SNR waveform utilising the dual-band capability. For the dual-band waveforms, we calculated the matched waveform for each band and then calculated the MI or SNR that the system expects to achieve on each band. The band with the better metric at that particular iteration was chosen for that transmission.

In this experiment, the TNR is set at 12 dB while the CNR is set to 9 dB. Fig. 9 shows the performances of the five waveforms. Notice that in the low-energy regime where the CR is noise limited rather than clutter limited, the SNR waveforms are very close in performance and the MI waveforms are close in performance. In the energy-rich regime (where clutter power is also stronger), both sets of waveform types converge to 0% misclassification error. Thus, the region in which there is performance gain is the region where there is separation of the performance curves. Expectedly, both dual-band waveforms performed well with dual-band MI performing the best. Interestingly, the wideband waveform performed the worst in low energy but overtook the single-band SNR and MI waveforms in high energy.

5.3 Waveform formation in multi-band application: Since the CR system was constrained to use a single band at a time, the system had to make decisions as to which band to use for a given transmission. The cycle of selecting a band and adapting the waveform that would be transmitted in that band continued until the experiment was terminated. The following figures detail the path taken by the dual-band MI waveform over a particular experiment, so chosen such that it had taken quite a few transmissions (93 transmissions in this case) to show waveform formation history. The true hypothesis was Target #4 shown in Figs. 7 and 8. The energy constraint for this trial was $E_s = 0.001$ (energy units) and the system made a decision after the 93rd transmission. Fig. 10 shows the MI calculations prior to waveform transmission. For the initial waveform, the MI calculation is greater for Band #2 and therefore the radar utilised this band as shown in Fig. 11. MI then became larger on Band #1 prior to transmission #5 and, thus, the radar switched to Band #1. A switch was again made to Band #2 at transmission #19 and the system finally settled on Band #1 at transmission #21, where it stayed until a correct decision was made. Fig. 12 indicates that the decision was Target #4 which was the true hypothesis. Fig. 12 also explains why the system required so many transmissions prior to making the right decision. Fig. 12 shows the probability update history. Since low transmit energy was used, confidence in the first set of probability updates are not high. In fact, Target #4 did not become the clear favourite until well after the 60th transmission.

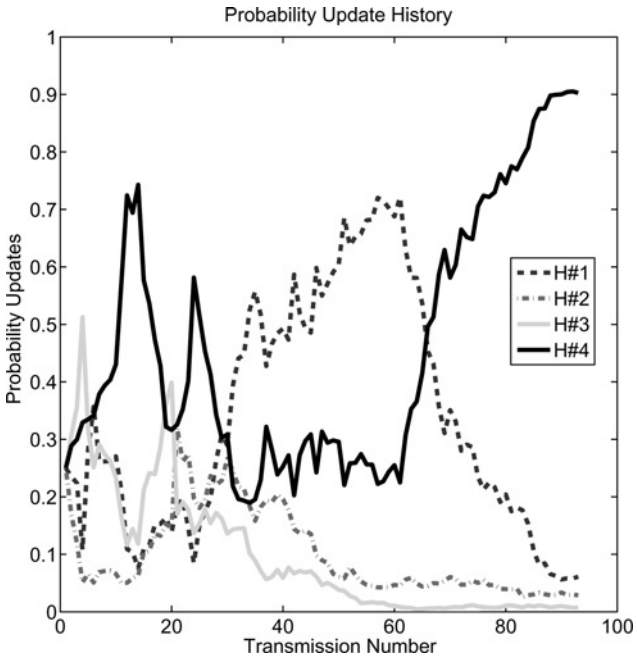

Figure 12 *Probability update history of the four hypotheses in a single experiment of dual-band CR*

6 Summary and conclusion

MI-based and SNR-based approaches to waveform design in signal-dependent interference and channel noise were investigated. Both waveform spectra can be obtained via a waterfilling operation on a function that depends on the target spectrum, the clutter PSD and the receiver noise

doi: 10.1049/iet-rsn.2008.0146

PSD. To maximise either MI or SNR, a radar system must customise the transmit waveform in such a way as to de-emphasise frequency bands where clutter is significant and emphasise frequency bands where clutter is negligible. A new analysis of the saturation of either MI or SNR with increasing transmit energy was also presented.

The proposed waveform designs were applied in a CR system where the objective was to identify a target from one of several possibilities using multiple transmissions in the presence of noise and clutter. We calculated a probability-weighted spectral variance over the target hypotheses and then used this variance for the target spectral variance needed by the waveform design techniques. Since the spectral variance over the ensemble depends on the hypothesis probabilities, the adaptive transmit waveform can be updated as the probabilities change in response to previous observations. Simulated results show that the waveforms perform well in terms of both error rate and the average number of transmissions required to make a decision. The clutter-compensated waveforms were, in general, the best performers.

7 Acknowledgment

The authors would like to thank Dr. Steven Kay for his helpful suggestion on using conditional-pdf approach in deriving the data pdf in the case of correlated target and/or clutter.

8 References

[1] HAYKIN S.: 'Cognitive radar: a way of the future', *IEEE Signal Process. Mag.*, 2006, **23**, (1), pp. 30–40

[2] BELL M.R.: 'Information theory and radar waveform design', *IEEE Trans. Inf. Theory*, 1993, **39**, (5), pp. 1578–1597

[3] PILLAI S., OH H., YOULA D., GUERCI J.: 'Optimum transmit-receiver design in the presence of signal-dependent interference and channel noise', *IEEE Trans. Inf. Theory*, 2000, **46**, (2), pp. 577–584

[4] KAY S.: 'Optimal signal design for detection of Gaussian point targets in stationary Gaussian clutter/reverberation', *IEEE J. Sel. Top. Signal Proc.*, 2007, **1**, (1), pp. 31–41

[5] DELONG J.D.F., HOFSTETTER E.M.: 'On the design of optimum radar waveforms for clutter rejection', *IEEE. Trans. Inf. Theory*, 1967, **IT-13**, (3), pp. 454–463

[6] YAZICI B., XIE G.: 'Wideband extended range-doppler imaging and waveform design in presence of clutter and noise', *IEEE Trans. Inf. Theory*, 2006, **52**, (10), pp. 4563–4580

[7] ESPOSITO R., SCHUMER M.: 'Probing linear filters-signal design for the detection probblem', *IEEE Trans. Inf. Theory*, 1970, **16**, (2), pp. 167–171

[8] MOSCA E.: 'Probing signal design for linear channel identification', *IEEE Trans. Inf. Theory*, 1972, **18**, (4), pp. 481–487

[9] GJESSING D.T.: 'Target adaptive matched illumination radar principles and applications' (Peter Peregrinus, London, UK, 1986)

[10] SOWELAM S.M., TEWFIK A.H.: 'Waveform selection in radar target classification', *IEEE Trans. Inf. Theory*, 1967, **IT-13**, (3), pp. 454–463

[11] ROMERO R., GOODMAN N.: 'Information theoretic matched waveform in signal dependent interference'. Proc. 2008 IEEE Radar Conf., Rome, Italy, May 2008, pp. 1–6

[12] GOODMAN N.A., VENKATA P.R., NEIFELD M.A.: 'Adaptive waveform design and sequential hypothesis testing for target recognition with active sensors', *IEEE J. Sel. Top. Signal. Proc.*, 2007, **1**, (1), pp. 105–113

[13] HYEONG-BAE J., GOODMAN N.: 'Adaptive waveforms for target class discrimination'. Proc. 2007 Waveform Diversity and Design Conf., Pisa, Italy, June 2007, pp. 395–399

9 Appendix: pdf derivation

The likelihood ratio between H_i and H_j after the Kth transmission and reception is

$$\lambda_{i,j}^{K} = \frac{p_i(\boldsymbol{y}_1, \ldots, \boldsymbol{y}_K)}{p_j(\boldsymbol{y}_1, \ldots, \boldsymbol{y}_K)} \frac{P_i^1}{P_j^1} \tag{56}$$

Thus, we require an expression for the joint pdf of the data conditioned on a particular hypothesis. If we define a joint pdf conditioned on the particular target realisation, then the joint pdf can be written as

$$p(\boldsymbol{y}_1, \ldots, \boldsymbol{y}_K) = \int_{\boldsymbol{g}} p(\boldsymbol{y}_1, \ldots, \boldsymbol{y}_k|\boldsymbol{g}) p(\boldsymbol{g})\, \mathrm{d}\boldsymbol{g} \tag{57}$$

For a single transmission, the pdf of the measurement $\boldsymbol{y}$, conditioned on $\boldsymbol{g}$, is

$$p(\boldsymbol{y}|\boldsymbol{g}) = \frac{1}{\pi^L |\boldsymbol{K}_N|} \exp\left[-(\boldsymbol{y} - \boldsymbol{X}\boldsymbol{g})^{\mathrm{H}} \boldsymbol{K}_N^{-1} (\boldsymbol{y} - \boldsymbol{X}\boldsymbol{g})\right] \tag{58}$$

Using this strategy, the measured data vectors for each transmission are independent when conditioned on the

target impulse response. Hence, we can write

$$p(\boldsymbol{y}_1, \ldots, \boldsymbol{y}_K|\boldsymbol{g}) = \prod_{k=1}^{K} p(\boldsymbol{y}_k|\boldsymbol{g}) \tag{59}$$

$$= \prod_{k=1}^{K} \frac{1}{\pi^L|\boldsymbol{K}_N|} \exp\left[-(\boldsymbol{y}_k - \boldsymbol{X}_k\boldsymbol{g})^{\mathrm{H}}\boldsymbol{K}_N^{-1}(\boldsymbol{y}_k - \boldsymbol{X}_k\boldsymbol{g})\right] \tag{60}$$

$$= \frac{1}{\pi^{LK}|\boldsymbol{K}_N|^K} \exp\left[-\sum_{k=1}^{K}(\boldsymbol{y}_k - \boldsymbol{X}_k\boldsymbol{g})^{\mathrm{H}}\boldsymbol{K}_N^{-1}(\boldsymbol{y}_k - \boldsymbol{X}_k\boldsymbol{g})\right] \tag{61}$$

Since $\boldsymbol{g}$ is zero-mean complex Gaussian, the pdf is

$$p(\boldsymbol{g}) = \frac{1}{\pi^L|\boldsymbol{K}_g|} \exp\left[-\boldsymbol{g}^{\mathrm{H}}\boldsymbol{K}_g^{-1}\boldsymbol{g}\right] \tag{62}$$

where $\boldsymbol{K}_g$ is the covariance matrix specific to the particular target class being evaluated. Expanding terms and accumulating them in the argument of the exponential, we have

$$\begin{aligned} &p(\boldsymbol{y}_1, \ldots, \boldsymbol{y}_K|\boldsymbol{g})p(\boldsymbol{g}) \\ &= \frac{1}{\pi^L|\boldsymbol{K}_g|}\frac{1}{\pi^{LK}|\boldsymbol{K}_N|^K} \exp\{-\boldsymbol{g}^{\mathrm{H}}\boldsymbol{K}_g^{-1}\boldsymbol{g} - \sum_{k=1}^{K}[\boldsymbol{y}_k^{\mathrm{H}}\boldsymbol{K}_N^{-1}\boldsymbol{y}_k \\ &\quad - \boldsymbol{y}_k^{\mathrm{H}}\boldsymbol{K}_N^{-1}\boldsymbol{X}_k\boldsymbol{g} - \boldsymbol{g}^{\mathrm{H}}\boldsymbol{X}_k^{\mathrm{H}}\boldsymbol{K}_N^{-1}\boldsymbol{y}_k + \boldsymbol{g}^{\mathrm{H}}\boldsymbol{X}_k^{\mathrm{H}}\boldsymbol{K}_N^{-1}\boldsymbol{X}_k\boldsymbol{g}]\} \\ &= \frac{1}{\pi^L|\boldsymbol{K}_g|}\frac{1}{\pi^{LK}|\boldsymbol{K}_N|^K} \exp\left[-\sum_{k=1}^{K}\boldsymbol{y}_k^{\mathrm{H}}\boldsymbol{K}_N^{-1}\boldsymbol{y}_k\right] \\ &\quad \times \exp\left[-\boldsymbol{g}^{\mathrm{H}}\left(\boldsymbol{K}_g^{-1} + \sum_{k=1}^{K}\boldsymbol{X}_k^{\mathrm{H}}\boldsymbol{K}_N^{-1}\boldsymbol{X}_k\right)\boldsymbol{g}\right] \\ &\quad \times \exp\left[\sum_{k=1}^{K}\boldsymbol{y}_k^{\mathrm{H}}\boldsymbol{K}_N^{-1}\boldsymbol{X}_k\boldsymbol{g} + \sum_{k=1}^{K}\boldsymbol{g}^{\mathrm{H}}\boldsymbol{X}_k^{\mathrm{H}}\boldsymbol{K}_N^{-1}\boldsymbol{y}_k\right] \end{aligned} \tag{63}$$

If we define the matrix

$$\boldsymbol{Q} = \boldsymbol{K}_g^{-1} + \sum_{k=1}^{K}\boldsymbol{X}_k^{\mathrm{H}}\boldsymbol{K}_N^{-1}\boldsymbol{X}_k \tag{64}$$

then we can complete the square such that we have

$$\begin{aligned} p(\boldsymbol{y}_1,\ldots,\boldsymbol{y}_K) &= E_{\boldsymbol{g}}[p(\boldsymbol{y}_1,\ldots,\boldsymbol{y}_K|\boldsymbol{g})] \\ &= \int_{\boldsymbol{g}} \frac{\pi^L|\boldsymbol{Q}^{-1}|}{\pi^L|\boldsymbol{K}_g|\pi^{LK}|\boldsymbol{K}_N|^K} \\ &\quad \times \exp\left[\sum_{k=1}^{K}\left[\boldsymbol{X}_k^{\mathrm{H}}\boldsymbol{K}_N{}^{-1}\boldsymbol{y}_k\right]^{\mathrm{H}}\boldsymbol{Q}^{-1}\sum_{k=1}^{K}\boldsymbol{X}_k^{\mathrm{H}}\boldsymbol{K}_N{}^{-1}\boldsymbol{y}_k\right] \\ &\quad \times \frac{1}{\pi^L|\boldsymbol{Q}^{-1}|}\exp\left(-[\boldsymbol{g}-\boldsymbol{z}]^{\mathrm{H}}\boldsymbol{Q}[\boldsymbol{g}-\boldsymbol{z}]\right)\mathrm{d}\boldsymbol{g} \end{aligned} \tag{65}$$

where

$$\boldsymbol{z} = \boldsymbol{Q}^{-1}\sum_{k=1}^{K}\boldsymbol{X}_k^{\mathrm{H}}\boldsymbol{K}_N^{-1}\boldsymbol{y}_k \tag{66}$$

The last line of (65) is the only part of the expression that depends on $\boldsymbol{g}$. Furthermore, this part of the expression is a Gaussian pdf with mean $\boldsymbol{z}$ and covariance $\boldsymbol{Q}^{-1}$. Thus, the joint pdf is

$$\begin{aligned} p(\boldsymbol{y}_1,\ldots,\boldsymbol{y}_K) &= \frac{|\boldsymbol{Q}^{-1}|}{|\boldsymbol{K}_g|\pi^{LK}|\boldsymbol{K}_N|^K}\exp\left[-\sum_{k=1}^{K}\boldsymbol{y}_k^{\mathrm{H}}\boldsymbol{K}_N^{-1}\boldsymbol{y}_k\right] \\ &\quad \times \exp\left[\left[\sum_{k=1}^{K}\boldsymbol{X}_k^{\mathrm{H}}\boldsymbol{K}_N^{-1}\boldsymbol{y}_k\right]^{\mathrm{H}}\boldsymbol{Q}^{-1}\sum_{k=1}^{K}\boldsymbol{X}_k^{\mathrm{H}}\boldsymbol{K}_N^{-1}\boldsymbol{y}_k\right] \end{aligned} \tag{67}$$

doi: 10.1049/iet-rsn.2008.0146